

Search for correlations between BATSE gamma-ray bursts and supernovae

J. Polcar^{1,2}, M. Topinka^{2,3}, D. Nečas⁴, R. Hudec², V. Hudcová², F. Hroch², N. Masetti⁵, G. Pizzichini⁵, and E. Palazzi⁵

¹ Astronomical Institute of the Academy of Sciences of Czech Republic, Ondřejov, Czech Republic
e-mail: polcar@physics.muni.cz

² Masaryk University Brno, Faculty of Science, Czech Republic

³ Max Planck Institute for Astrophysics, Box 1317, 85741 Garching, Germany
e-mail: toast@asu.cas.cz

⁴ Brno University of Technology, Faculty of Civil Engineering, Czech Republic

⁵ I.N.A.F. Istituto di Astrofisica Spaziale e Fisica Cosmica, Sezione di Bologna, Via Gobetti 101, 40129, Italy*

Received 7 June 2005 / Accepted 14 February 2006

ABSTRACT

We report on our statistical research of space-time correlated supernovae and CGRO-BATSE gamma-ray bursts. There exists a significantly higher abundance of core-collapse supernovae among the correlated supernovae, but the subset of all correlated objects does not seem to be physically different from the whole set. The upper limit of the fraction of possibly correlated GRBs and SNe is of order of a few percent.

Key words. gamma rays: bursts – stars: supernovae: general – methods: statistical

1. Introduction

1.1. Motivation

The origin and sources of gamma-ray bursts (GRBs) still remain a puzzle. It is generally supposed that their tremendous energy could be released on a short time-scale during a collapse of a massive star in a supernova-like explosion (e.g. Rees & Meszaros 1992). There exist several pieces of indirect observational evidence supporting the connection between the GRBs and the supernovae (SNe):

- There is, of course, a famous coincidence in space and time between GRB 980425 and SN 1998bw. The probability of this coincidence just by chance is of the order of 10^{-4} (Galama et al. 1998). Since that time we have seen even stronger coincidence in the case of GRB 030329 and SN 2003dh (Staneke et al. 2003; Hjorth et al. 2003).
- Several GRBs reveal a bump – a rebrightening – in a late optical afterglow lightcurve (e.g. GRB 980326) (Bloom 1999), it resembles an underlying SN (Galama et al. 2000). A recent study shows that there could be a sign of an underlying SN in all GRB optical afterglows of redshift less than 0.7 (Zeh et al. 2005).
- Sometimes we can see SN-like spectral and color indices behavior (e.g. GRB 030329 and SN 2003dh), in some cases X-ray afterglow spectra show the presence of Fe (e.g. GRB 991216, GRB 000214, GRB 990705) (Piro et al. 2000) or other metal lines (e.g. GRB 011211) (Metger 1997) being also typical for SNe, but is not conclusive. Note, that the existence of intensive and narrow Fe line requires a SN explosion before the GRB (Vietri & Stella 1998).

- High column density in the circumburst medium around some GRBs as well as irregularity of blue host galaxies also indicate that GRBs could originate in star-burst regions or star-forming galaxies (Bloom et al. 2002). But the distribution of GRB radial distance from the center of the host galaxy proved no positive correlation with SNe (Tsvetkov 2001; Blinnikov et al. 2000).
- The energetic balance and the GRB rate, both corrected for a narrow collimation factor, yield a number of the order being comparable to the order of the SNe number (Frail 2001).

We know that the distribution GRBs' duration is bimodal (Kouvelioutou 1993), dividing the GRBs into two groups: the one of long durations (>2 s) and the other one of short ones (<2 s). Due to the technical limits short GRBs are more difficult to detect and localize, therefore no afterglow of a short GRB has been detected yet (Matheson 2004) regardless whether these exist or not¹. Neither it is not theoretically clear if the short GRB can be produced in a SN-like explosion. Thus all the statements above are valid for long GRBs only and we cannot a priori say anything on the correlation between the short GRBs and the SNe.

1.2. Previous work

Supernovae have been associated with GRB since Colgate's model (Colgate 1974) which had been proposed during the time of the discovery of the bursts. In recent years, models have been proposed that GRBs are a collapse of a massive star, which should also produce a SN. It is believed that massive stars can produce a variety of energetic explosions ranging from traditional supernovae to energetic GRBs, and seemingly all points

¹ Very recently there is a new report of an optical afterglow observation for a short burst GRB 050509B (Bloom et al. 2005).

* Formerly IASF/CNR Bologna.

in between. On the other hand, ordinary SNe come from neutron star formation in a spherical explosion of a massive (more than 8 solar masses) star with little or no fall back. Failed or weak explosions in rotating stars give hyper-accreting black holes whose jets can both explode a star in a grossly asymmetric way and produce a variety of high energy phenomena. Collapsar is a black hole formed by the incomplete explosion of a rapidly rotating massive star (Woosley 1993). In such a scenario, SN is produced by every GRB, but not every SN produces a GRB. It is assumed that the long duration GRBs are caused by the core collapse of a massive fast rotating star with a massive accretion disk around the forming black hole and a jet which bursts out through the infalling material to appear as a GRB to an observer within the beam. In such a case, all long duration GRBs should have a SN appearing in the following month or so. This is however difficult to observe since e.g. for the distance of $z = 1$ the underlying SN would peak at magnitude 25 roughly 20 days after the burst. So the SN will only appear as an inflection in decline of the afterglow and can hardly be convincingly identified.

The various aspects of the SN-GRB relation have been intensively studied and debated during past years. There is a growing evidence (both direct and indirect) for SN-GRB association (see e.g. Dar 2004 and Zeh et al. 2004, for a review). There are very important cosmological implications. If GRBs are indeed associated with SNe, then the first bursts should have occurred shortly after the first stars formed, at redshifts of $z \sim 15-20$. Bursts and their afterglows should be indeed observable out to these very high redshifts. GRBs can hence serve as a probe for the early Universe – beacons to locate core-collapse SNe at very high z and to study the properties of these SNe.

In this work, we focus on the analysis of possible time and positional coincidences between catalogued SNe and catalogued GRBs. Several analogous studies were published in the past (e.g. Kippen et al. 1998; Wang & Wheeler 1998) however, in our opinion, none of them was general and complex (or statistically treated in a complete proper way). We consider in the present work all known SNe without any restriction since, in our opinion, any limitation would be in contrast with the main goal (complex statistical approach) of the study.

In detail, the study of Kippen et al. (1998) was restricted to brighter events only (brighter than mag 17) but this is in contrast with the observed OA statistics (their peaks are fainter than 17 mag in most cases) while Wang & Wheeler (1998) restrict to SNe of known Ia, Ib types (but the OA may be also among weak and unclassified SNe). In our understanding, any complex study should take into account that the statistical significance of the results of cross-correlations between the GRBs and SNe is affected and limited by the following: 1) the positional uncertainty of a quite large fraction of the GRBs is high; 2) the dates of SN peaks in most cases are unknown; 3) the results of optical SNe searches do not represent a full and homogeneous sample so that many (and even a large majority) of the SNe may be missed especially at faint magnitudes; 4) also the BATSE GRB catalog we used (i.e., the one of BASTE, see Sect. 2.1 does not represent the full and complete GRB sample since not all GRBs were detected by this instrument; and 5) there is no systematic sky patrol survey at magnitudes below 15 – i.e. the SNe found so far and included in the SN catalogues are not found by all sky deep patrol but rather by searches focusing on small pre-selected areas of the sky, hence the SN catalogues include only a very small fraction of SNe in the observable universe (Hudec et al. 1999; Dar 2004; Zeh et al. 2004).

In the previous work by our group in this direction (e.g. Hudec et al. 1999, 2001), we provided the basic cross-correlation

(however, with no complex statistical approach) with the goal to study in detail the parameters and properties of the correlated pair objects found. We do not repeat this approach here. These obvious limitations following from this analysis were due to the incomplete and/or poor data especially for faint SNe.

For the correlations found, most of the related SNe represent poorly investigated events with poorly known (and in many cases even completely unknown) light curves, decline rates, color indexes and no or limited spectral information, hence the decision whether they could be related to the GRBs in question is difficult. The recent detections of faint OA of GRBs strongly support and justify further extended and more complete searches for new faint and variable optical objects especially at faint magnitudes (18 and more).

Some of this information can be retrieved from deep archival plates (some of the archival plate collections reach the limiting magnitudes of 20 and even 23 such as ROE Edinburgh and TLS Tautenburg, e.g. Hudec 1999) but a systematic deep CCD patrol could provide more precise and much more complete database.

In the present work, we focus on complex and careful statistical treatment of the cross-correlated catalogs. This is a difficult task due to large positional inaccuracies of the large BATSE GRB catalog and other influences such as the incompleteness of the recent SNe catalogue – despite the fact that the number of yearly detections of SNe is growing, the detection rate is still very far from the estimate of about 10^6 SN explosions in the observable universe per day (Dar 2004). More accurately, the rate of type Ib-Ic-II SNe has been estimated from their observed rate in the local Universe (e.g. Van den Bergh & Tammann 1991) and the star formation rate as function of the redshift, to be $\sim 10 \text{ s}^{-1}$ in the observable Universe (Madau 1998).

1.3. The lesser number of well-localized GRBs against the greater number of poorly-localized GRBs

Till today (May 2005) there are about 285 well-localized GRBs detected but only 27% of them have an optical afterglow observed (Greiner 2004) and only in cases of GRB 980425 with SN 1998bw, GRB 030329 with SN 2003dh and GRB 031203 with SN 2003lw (Gal-Yam et al. 2003; Malesani et al. 2004) the correlation with a SN is more or less evident. Around 30% (Greiner 2004) of GRBs are so called dark bursts with X-ray but no optical afterglow detected even when followed by rapid and deep Earth-based observation (Jakobsson et al. 2004).

A natural question arises why we do not see the sign of an underlying SN to every rapid well-localized GRB observation and vice versa. It may imply that only a fraction or a subclass of GRBs is connected to SNe and vice versa. Because the number of well-localized GRBs with the optical afterglow is statistically small we decided to use a different approach. We left away the idea of analyzing each single possibly correlated GRB or each possibly correlated SN case by case; rather, we made a search for coincidences of GRBs and SNe in space and in time and we analyzed the results instead. We then looked for the correlation investigating the statistical properties of the coinciding pairs.

2. Input data sample

2.1. GRB catalogue

We used the largest available complete catalogue of GRBs, the current CGRO-BATSE GRB catalogue (the version from April 2004) (BATSE²) that provides calibrated data from the BATSE

² BATSE catalogue <http://coss.gsfc.nasa.gov/batse/index.html>

Table 1. Spectrum of SNe pseudotypes in matched SNe. Symbol \mathbb{A} indicates pseudotypes independent matching, \mathbb{B} sign matching with respect to SNe pseudotypes. The number in parenthesis shows the number of SN–GRB matched pairs in the match. N_{BATSE} gives the number of all SN of each pseudotype in the BATSE era. The influence of the SN pseudotype on the match and the motivation for introducing two sets of matching parameters \mathbb{A} and \mathbb{B} is given with a detailed explanation in Sect. 3.2.6.

pseudotyp	$\mathbb{A}(81)$	$\mathbb{A}(81)$ [%]	$\mathbb{B}(105)$	$\mathbb{B}(105)$ [%]	N_{BATSE}	N_{BATSE} [%]
unknown	6	7.4	14	13.3	312	30.9
core	37	45.7	52	49.5	263	26.0
dwarf	38	46.9	39	37.1	435	43.1

experiment. It covers the time period of almost 10 years, from 1991 to 2000. For the purposes of our analysis we extracted the unique GRB ID, the coordinates, the size of errorbox, the time of detection, the duration in terms of T_{90} , the fluxes in 64 s, 256 s and 1024 s integration time-scale and the fluences f_i for all four channels (1: 20–50 keV, 2: 50–100 keV, 3: 100–300 keV and 4: >300 keV). The catalogue consists of 2707 GRBs.

2.2. SN catalogues

The input data for the SNe were taken from the Harvard CFA³ and the Sternberg SAI⁴ catalogue of SNe. We combined the data and we used the following properties of the SNe: the unique ID, time of discovery, the coordinates, visual magnitude at the time of discovery, the relative offset from the host galaxy, the type of the SN, the time of the maximum of the optical lightcurve and the redshift. For the SNe with known redshift we derived the radial distance from the center of the host galaxy r and the absolute visual magnitude M using the following cosmological parameters ($H_0 = 70 \text{ km s}^{-1} \text{ Mpc}^{-1}$, $\Omega_m = 0.3$, $\Omega_\Lambda = 0.7$) for luminosity distance d_L calculation. The total number of SNe is 2871, 2803 of them are provided with at least partial information, 1010 of them in the BATSE era. None of the SN with no detailed information belongs to the BATSE era.

2.3. Pseudotypes

There is a wide range of SN types in the input data. For easier manipulation and mainly for better control over the matching parameters in the search for correlation (for further explanation of \mathbb{A} and \mathbb{B} see later Sect. 3.2.6) we divided all the SNe into several types, we call them pseudotypes. The abundance of pseudotypes in the set of the SNe is listed in Table 1. Note that the division is not disjunctive. For the purposes of our study it is useful to simplify this division into three pseudotypes only: the dwarf, the core and the unknown SNe (typewriter font is used for pseudotype names.)

The dwarf SN is a SN deriving its physical origin from the explosion of a white dwarf due to accretion of matter in a binary system. It usually manifests as a type Ia SN. This kind of SN has no theoretical or experimental reason to be linked with a GRB.

The core SN we call the SN which is believed to have its origin in the collapse of the core of the single star into a neutron star or/and a black hole. This simply covers the rest of the

known types. At least some of these SNe could be theoretically connected with GRBs.

The last type, the unknown SNe are the unclassified SNe we have no information about the type. Of course, some of these SNe could be also physically correlated with GRBs.

3. Search for the correlation

3.1. Introduction

We created a database from the selected catalogues and we matched the catalogues to look for the space and time coincidences. A SN and a GRB are matched together if they coincide both in the space and in the time domain (see Sect. 3.2).

3.2. Determining matching parameters

3.2.1. The space domain

The situation is easy in the space domain: a GRB and a SN make a pair if the location of the SN falls into the GRB errorbox which yields 3σ error.

3.2.2. The time domain

In the time domain it is not a priori theoretically clear what is the time delay between an eventual gamma-ray emission which could be interpreted as a GRB and the optical emission observed as a SN. For our simplicity we postulated the time of the optical emission to be the time of the maximum T_{max} of the optical lightcurve of the SN.

Unfortunately only a tiny fraction of all SNe provides an information about the date of the maximum T_{max} (0.14%). We solved this problem statistically and we assumed the time delay between the time of the maximum T_{max} and the time of the discovery T_{disc} to be the median $M_{\text{max}} = -4$ days of the distribution of all time delays between the time of maximum and the time of the discovery wherever it is known (see the plot in the Fig. 1). Thus for the SNe for which the time of the maximum is missing we computed it as $T_{\text{max}} = T_{\text{disc}} + M_{\text{max}}$. The value of the median does not differ significantly (± 1) day for dwarf and core pseudotypes.

The time delay $T_\delta \equiv T_\gamma - T_{\text{max}}$ between possible prompt gamma emission T_γ of the SN and its optical emission T_{max} may depend on the type of the SN. The positive time-shift means that the optical emission comes later than the gamma emission, the negative means the opposite. We take this into account during the division into pseudotypes. We represent the time delay T_δ as the Gaussian fit of the distribution of the time delays within the pseudotype. It is characterized by two values: the mean value μ_γ for the mean time shift and the half-width of the time window T_{error} which is Gaussian $3\sigma_\gamma$ error. Generally this could be written as

$$T_\gamma = (T_{\text{max}} + \mu_\gamma) \pm 3\sigma_\gamma.$$

We tried to make the best possible estimate of the time-window parameters for each pseudotype.

3.2.3. Dwarf supernovae

Mainly because of the usage of the SNe of the type Ia as the cosmological lighthouses, these are already well understood and

³ Harvard a Smithsonian Observatory <http://cfa-www.harvard.edu/iau/lists/Supernovae.html>

⁴ Sternberg Astronomical Institute <http://www.sai.msu.ru/sn/>

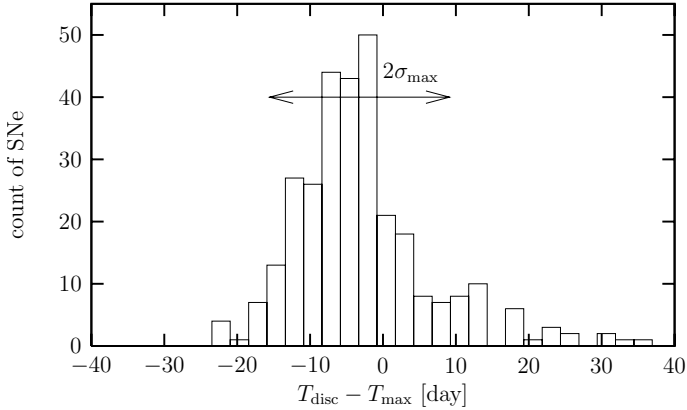


Fig. 1. Histogram of time delays between maximum SNe and its discovery for all the SNe where the data are available.

several templates of type Ia SNe are known. The typical time delay T_δ can be estimated for the dwarf SN as a relatively narrow time interval $T_\gamma = (T_{\max} - 20 \pm 7)$ days (Petschek 1996).

3.2.4. Core supernovae

In the case of core SNe the estimation of the time delay T_δ is more problematic. For a classical SN we expect that the high energetic photons can escape the exploding envelope of SN earlier than the less energetic photons at the optical wavelengths. Although there is a progress in understanding the models and simulations of the SN core-collapse were made (Janka & Rufert 1999; MacFayeden et al. 1999; Drago et al. 2000), the time delay is not theoretically known. The exact value is a complicated and very sensitive function of the star mass, the metallicity, the circumstellar environment, the rotational and electromagnetic properties of the star and, of course, it depends on the used model. We do not know these parameters and their calculation would be far beyond the scope of this paper. There exist several observations of a core-collapse SN in which the time delay between gamma and optical emission is around 14 days (Koshut 1996).

We chose the typical values of the time delay to be $T_\gamma = (T_{\max} - 0 \pm 30)$ days. The negative time shift corresponds to the possibility of a supranova model as well (Vietri & Stella 1998). In the supranova model the SN first explodes and then it leaves a rotating neutron star. After the system reaching the critical value of energy, the remnant collapses into a black hole. Then, during the second explosion, a GRB could be produced.

Both sides of the range of the time interval could be theoretically extended up to several months, even years if special initial conditions of the core-collapse system are used, but a larger time window than about ± 1 month would erase all correlations due to the statistical errors. Note that we assume only a small fraction of correlated pairs to be found, if any.

3.2.5. Unknown or uncertain supernovae

For the SNe of unknown or uncertainly determined type we used a statistical estimation of the time-shift and of the width of the time-error. Another uncertainty lays in the T_{\max} estimation. All this is described by the magic_x number (see Table 2). The larger uncertainty, the larger the time window is. For each pseudotype we assume the Gaussian distribution of the probability of the time delays T_δ . We calculated the weighted average of all

Table 2. The explanation of magic_x parameter and the number of counts of SNe.

magic_x	#SNe	#SN _{BATSE}	sense
0	68	68	unknown discovery time \Rightarrow no knowledge
1	1056	238	statistically guess t_{\max} , unknown type
3	107	9	sure of t_{\max} , unknown type
5	108	39	statistically guess t_{\max} , unsure type
7	8	5	sure of t_{\max} , unsure type
13	1245	540	statistically guess t_{\max} , sure of type
15	279	107	sure of t_{\max} , sure of type

Table 3. Used time window intervals for each SN pseudotype and magic_x .

magic_x	Δ_{core} [day]	Δ_{dwarf} [day]	Δ_{unknown} [day]
0	–	–	–
1	–	–	[–24; 53]
13	[–67; 67]	[–24; 64]	–
15	[–30; 30]	[18; 22]	–
3	–	–	[–24; 61]
5	[–61; 74]	[–51; 85]	–
7	[–27; 36]	[–23; 61]	–

contributing densities of the probability for every configuration of the magic_x with respect to the level of uncertainty we had in determining the SN properties. As the weight we used the abundance of the pseudotype in the catalogue. For the match we used the best Gaussian fit of the sum of the probability densities. We summarized the values of the parameters used in the match in the Table 3. A graphical representation of the building of the time-delay probabilities is shown in Fig. 2.

3.2.6. Two sets of matching parameters

Not all the SNe have their type defined, some of them are defined with doubts. Some of the SNe could also have been classified inaccurately. Of course, there also is a non-zero probability that a small fraction of faint SNe has been misclassified at all and these SNe were unrecognized GRB optical afterglows (Hudec et al. 2001). The matching process itself reflects the effect of the division of the SNe into the pseudotypes. It results in the different size of the time window and in the different expected value of the matched pairs used for each pseudotype. The larger time errorbox of the particular pseudotype is, the greater number of matched pairs of this kind. To measure this effect it is useful to do the matching separately for two different sets of parameter settings: we denote \mathbb{A} for the parameter set which is independent on the pseudotype of the SN and \mathbb{B} for which is not.

While in the case \mathbb{A} we used the values described above, for \mathbb{B} we used the constant time delay $T_\gamma = (T_{\max} - 0 \pm 30)$ days regardless of the pseudotype. It agrees with the fact that the bump in the optical afterglow usually appears within several days or weeks after the burst (Greiner 2004). However, this is a one-way limit. The negative boundary covers the possibility that the optical emission precedes the gamma phase, e.g. in a prompt preburst optical emission of GRB (Paczynski 2001) or the supranova model of GRB (Vietri 1998).

We notice, that due to the nature of the GRB detection, it is not possible to monitor the entire sky continuously and a “beforeglow” has been never seen. But it does not reject the possibility of any preburst optical emission and the negative time delay is worth to be assumed as well.

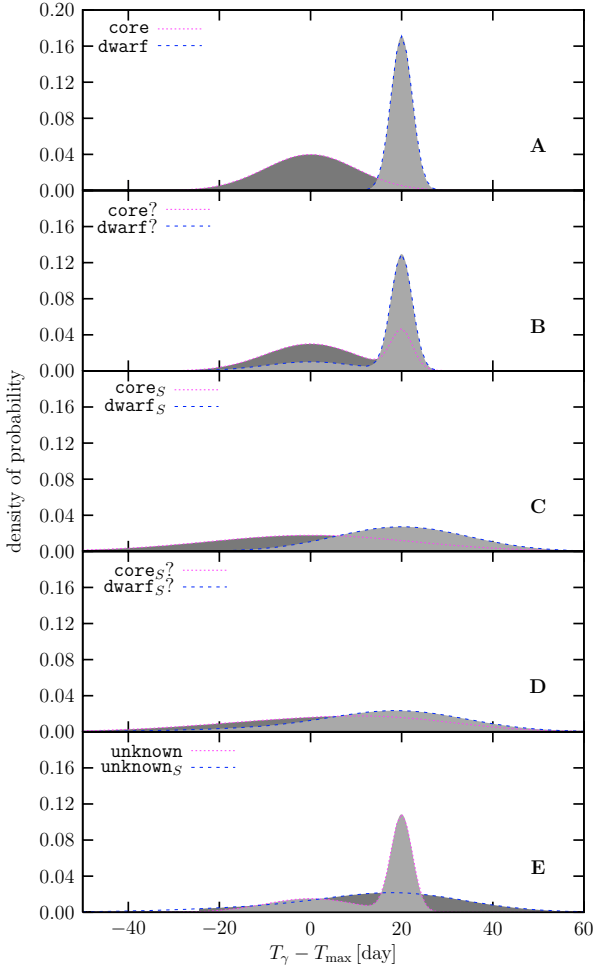


Fig. 2. Composite density of the probability of the time delay between the gamma emission and the maximum of the optical emission for SNe for which the type is uncertain (?), determined statistically (S) or unknown. The resulting Gaussian fit of the weighted average is shown (filled).

For both **A** and **B** a change of the width of the time window in the interval of the value of 60 days effects the number of matched pairs linearly. We investigated that there is no critical or preferred value up to the size of the time window of ~ 100 days, see the Fig. 3.

4. The match itself and analysis of the results

4.1. Correlation in space and in time

4.1.1. Theory

The missing part of many similar studies is the discussion of the obtained number of possibly correlated pairs. If we take one particular GRB randomly, the probability that there is a SN inside the errorbox of the chosen GRB within the given constant time window is

$$P_{\text{GRB-SN}} = P_{\text{phys}} + P_{\text{rand}} - P_{\text{phys}}P_{\text{rand}}$$

where P_{phys} is the probability that the GRB falls into the errorbox because of the real physical correlation, and P_{rand} is the probability of the random coincidence P_{rand} .

We assume that only a fraction f of GRBs and SNe is physically correlated. If we could have an ideal observation with no

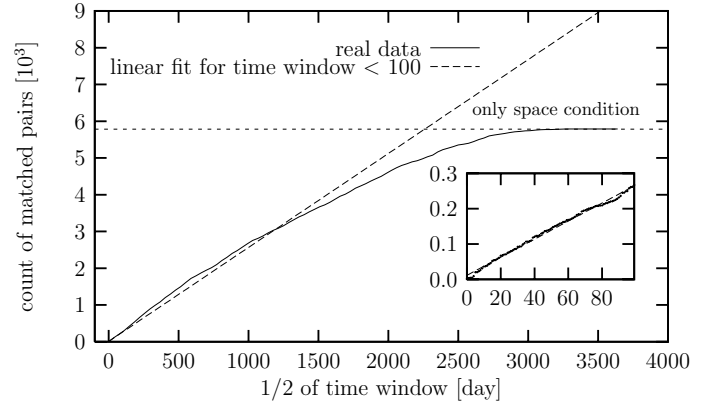


Fig. 3. Effect of time window size for count of matched GRB-SNe pairs.

limits, we would have seen a SN to every *correlated* GRB (if any and vice versa) and we would get $P_{\text{phys}} = f$.

But the reality is that a SN could be too faint to be observed (due to the extinction in the galactic plane, bad weather conditions, detector limits etc.) A GRB could also be out of the BATSE detector range or out of its field of view. Note, that at one time BATSE can cover about 50% of the sky and the GRB is a rapid and transient event. Since the angular distribution and the detection rate of GRBs are isotropic, the angular distribution of SNe is far from being isotropic (due to the absence of complete sky SN survey, the obscurity with the galactic plane, several campaigns run, etc.) The detection rate of SNe is not isotropic but exponential in time.

4.1.2. Catalogue rotation

Due to the limits of non-ideal observation the probability $P_{\text{GRB-SN}}$ of finding a SN within the errorbox of the chosen GRB is not the same as the probability $P_{\text{SN-GRB}}$ of finding a GRB with a proper errorbox for the chosen SN. Even more none of these probabilities yield the expected number of the matched pairs in the terms of the matching criteria described above.

It would be useful to compare results of the real match with an artificial match between a GRB catalogue and a SN catalogues where is no physical correlation ad hoc. The best method to generate such catalogues of the same statistical properties is to take the original GRB one and rotate the GRB coordinates along the all three axis for (α, β, γ) in the term of Euler angles. Thus we generated artificial GRB coordinates uniformly according to the isotropic distribution of the GRBs. By this technique we erase all the physical correlation artificially, if any, but the statistical properties remains unchanged. Note, that we need one catalogue to be isotropic, in our case the GRB one.

4.2. Number of pairs

4.2.1. Theory

First we compared the number of the pairs from the real match with the mean result of the matches between artificial catalogues generated using the rotation method over different values of the rotation angles (α, β, γ) . If there exists an additional physical correlation apart from the random one, the number of matched pairs will be higher in average when the real data set is used.

The question is how small the correlation factor f could be to be detectable by this method. To test this we created artificial

Table 4. Summary of multiple matched SNe and GRBs. Symbol **A** describes SN pseudotype independent match and **B** describes matching with respect to SN pseudotype. In the bracket are counts of unique appearance of object in matched pairs.

appearance	A		B	
	SNe(81)	GRBs(77)	SNe(105)	GRBs(99)
7×	–	–	–	1
6×	–	–	–	1
5×	–	–	–	1
4×	–	1	–	1
3×	1	2	2	1
2×	9	8	18	12
1×	71	66	85	82

Table 5. Compare result of matching SN pseudotype independent match (**A**) and matching with respect to SN pseudotype (**B**).

77	pairs are in both matches, A and B
15	pairs of A are not include in B
50	pairs of B are not include in A
8	GRBs of A pairs are not include in B pairs
31	GRBs of B pairs are not include in A pairs
14	SNe of A pairs are not include in B pairs
40	SNe of B pairs are not include in A pairs

data set in the term of the catalogue rotation. The GRB errorboxes were taken a) randomly from the distribution of the real GRB errorboxes b) to be the median of the GRB errorbox distribution. (We denote the distribution of the errorboxes as ρ .) Then a fraction p of GRBs is set to be artificially correlated to a randomly chosen (but unique) SN in the meaning of the space and time condition used in the real matches **A** and **B**. The values of p ran from $p = 0$ (no correlation) to $p = 0.14$. We can see the average number of the matched pairs in the artificial catalogues as well the 1σ errorbars. The cross-section of the errorbars with the constant number of the pairs found in the real match shows the limit put on our search.

4.2.2. Results

The results of real matching we had run for the set of the parameters **A** and **B** are listed in Tables 4 and 5. We obtained 92 of possibly correlated pairs in the case **A** and 127 in the case **B**. The sky maps illustrating the results are plotted in Figs. 4 and 5. Difference between **A** and **B** case are described in Table 5. Multiple matched GRBs and SNe are summarized in Table 4. The histogram of results of the match for 295 rotations both for **A** set of the parameters is shown in Fig. 15.

In both cases we found that the number of matched pairs is less than the average number of matched pairs as they were derived from the rotations, but in both cases (**A** and **B**) they lay within 1σ error.

The detailed view in the Fig. 6 shows that in the case a) if there is any correlation, it is close to $p \sim 0$ for both **A** and **B** in the meaning of 1σ . In the **B** case the number of pairs from the real match is even below 1σ of zero number of the coincidences. If we enlarged the errorbars to 3σ we get the maximal value of the fraction of the physically correlated pairs $p \sim 0.008$ both for **A** and **B**. In the case b) (Fig. 7) we got the limits $p \sim 0.011$, resp. $p \sim 0.015$ for **A**, resp. **B** in the meaning of 1σ . We got $p \sim 0.018$ resp. $p \sim 0.022$ for **A** resp. **B**.

But the zero point in the case b) is shifted against the completely disrupted data in the meaning of the mean of the

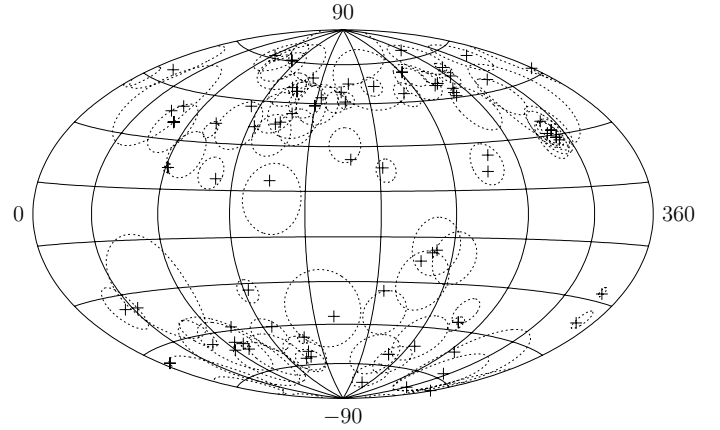


Fig. 4. Matched GRB–SNe pairs for the case **A** independent on SNe pseudotypes.

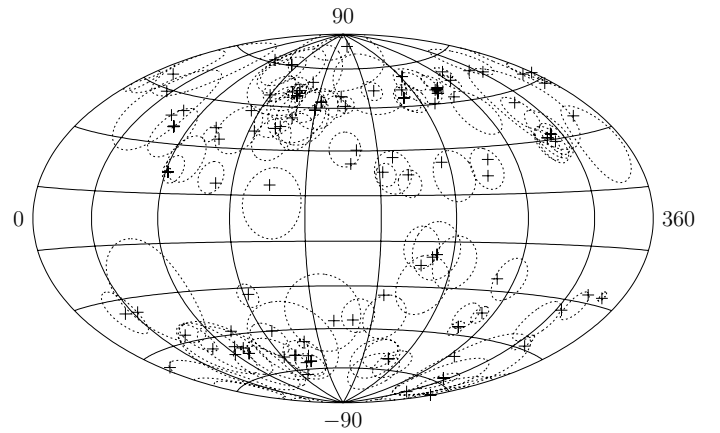


Fig. 5. Matched GRB–SNe pairs with respect to SNe pseudotypes – the case **B**.

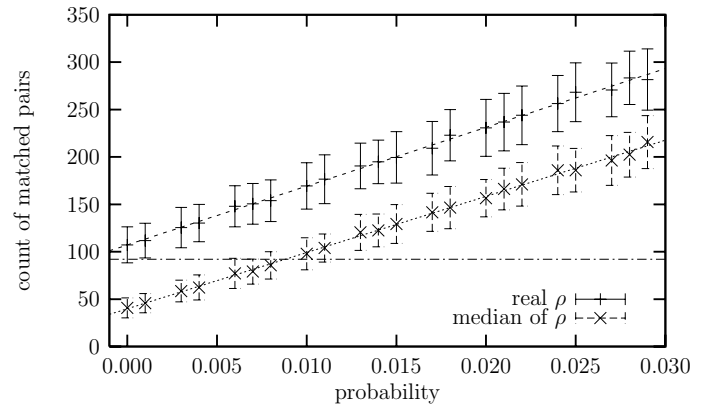


Fig. 6. Simulation of GRB–SNe pairs matching for defined artificial coincidence, SNe pseudotypes independent case. Horizontal line shows count of real matched pairs.

distribution of the catalogue rotations. The shift is caused by the difference between the mean errorbox and the median errorbox.

We checked whether there is a higher abundance of the pairs with the core SN in which the optical SN emission precedes the GRB (corresponding to the supranova model) or the opposite (classical collapsar scenario). There is only a slight preference of the collapsar model $N_{\text{collapsar}}/N_{\text{supranova}} \sim 1.3$, but it is not significantly high enough to reject the supranova model neither

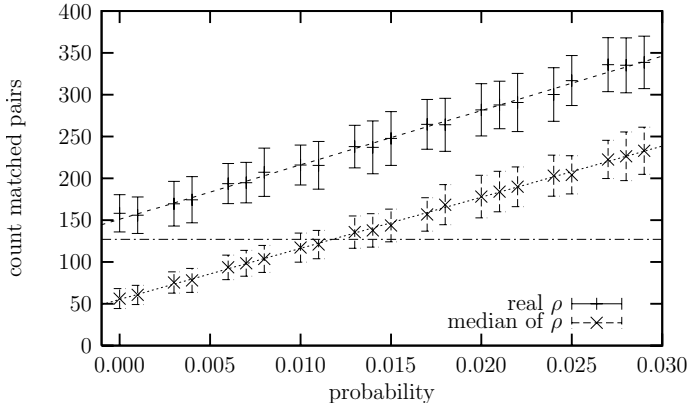


Fig. 7. Simulation of GRB–SNe pairs matching for defined artificial coincidence with respect to SNe pseudotypes. Horizontal line shows count of real matched pairs.

to prove the collapsar model. For the more detailed discussion see (Topinka & Polcar 2006).

4.3. Correlation tests

4.3.1. Theory

We assume that if there exist any physically connected pairs of GRBs and SNe, then the physical properties of these GRBs and these SNe are not independent. It is useful to test it. We generated two sets of artificial data again, the set of GRBs and SNe with a fraction of artificially created pairs, where one of the physical properties from the first catalogue is artificially correlated with another from the second catalogue by setting a polynomial dependence between them. For correlation coefficient K_{corr} of two random values ξ_1 and ξ_2 we can write

$$K_{\text{corr}}(\xi_1, \xi_2) = \frac{D(\xi_1, \xi_2)}{\sigma_1 \sigma_2}$$

where

$$D(\xi_1, \xi_2) = E(\xi_1, \xi_2) - E(\xi_1)E(\xi_2)$$

($E(\xi)$ is mean value of ξ), σ_1 is dispersion of random value ξ_1 and σ_2 is dispersion of random value ξ_2 . Correlation coefficient is from interval $[-1, 1]$, value $K_{\text{corr}}(\xi_1, \xi_2) = 0$ means uncorrelated random values ξ_1 and ξ_2 , value $|K_{\text{corr}}(\xi_1, \xi_2)| = 1$ means fully correlated ξ_1 and ξ_2 .

4.3.2. Results

We searched for the correlation between the physical properties of the matched GRBs and the matched SNe in the term of the correlation test described above. We compared the result of the test between the real data and a sample of artificially made pairs created by the catalogue rotations. We achieved the Gaussian fit for each correlation distribution.

The physical quantities of the highest absolute values of the correlation coefficient K_{corr} are listed in the Table 6 for the case **A** and in the Table 7 for the case **B**, the corresponding plots of the density probabilities of K_{corr} for the random generated GRBs and SNe is shown in Fig. 8 for **A** (the plot for **B** is not shown). The K_{corr} for the real data is marked by the dashed vertical line.

For the purposes of these tests we assumed that the GRB and the SN in the pair share their properties together, e.g. the SN redshift becomes the GRB redshift as well. These properties are not independent anymore.

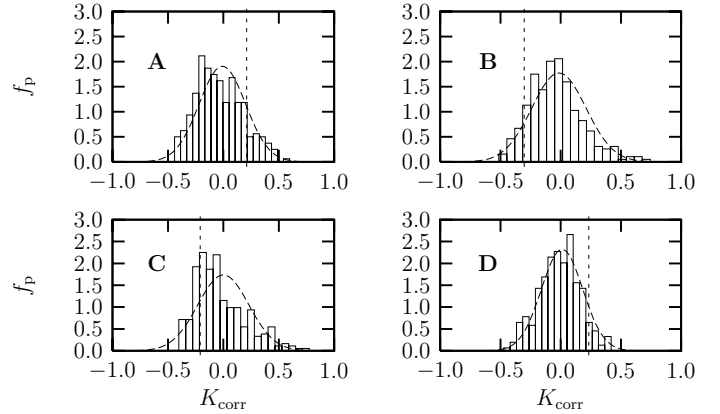


Fig. 8. Density of probability of most correlated quantity of matched pairs of random GRB–SN. Vertical dashed lines shows real K_{corr} .

Table 6. Results and parameters of the Gaussian fit for the correlation tests between the GRB/SN quantities in the matched pairs (case **A**).

Fig. 8	SNe q.	GRB q.	K_{corr}	μ	σ
A	m	h2s	0.211	-0.0087	0.209
B	r	F_{64}	-0.302	-0.0141	0.225
C	r	f_3	-0.208	0.0001	0.230
D	M	T_{90}	0.234	0.0119	0.171

Table 7. Results and parameters of the Gaussian fit for the correlation tests between the GRB/SN quantities in the matched pairs (case **B**).

SNe q.	GRB q.	K_{corr}	μ	σ
r	F_{64}	-0.249	-0.0056	0.181
d_L	f_2	0.225	-0.0131	0.178
r	f_3	-0.217	-0.0128	0.190
r	f_2	-0.188	-0.0030	0.196

The values obtained from the non-rotated real pairs are normal within 3σ , which is of 99.7% significant level even for the most correlated quantities. If there were any physically correlated objects among the matched pairs they would not affect their partner in the pair dramatically.

The relatively high value of the correlation coefficient K_{corr} found in some cases does not seem to have any physical reason in case of correlation e.g. between the distance of the SN from the center of its host galaxy r and GRB flux F_{64} . The correlation test did not prove any positive or negative correlation.

4.4. Short versus long

4.4.1. Theory

We tested the sub-sample of the matched pairs on the ratio of short to long GRBs among the possibly correlated pairs with respect to the whole sample of all GRBs from BATSE. It is believed that the short GRBs are of different physical origin from the long GRBs. Both of the two examples of GRB–SN correlation (SN 1998bw and SN 2003dh) as well as the other suspicious GRBs with the signs of an underlying SN observed are connected to the long GRBs. We cannot say if it is due to the selection effect or if it is because of their physical nature.

We split the GRBs into two groups according to their T_{90} . We made the rotation test again and investigated whether the ratio between the short and the long ones differs from the real match case.

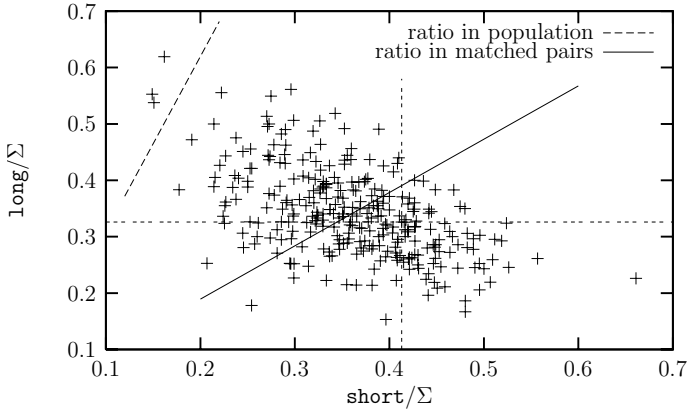


Fig. 9. Fraction of short and long GRBs in matching simulation. Horizontal and vertical dashed lines shows point of ratio for real matched pairs of GRB–SNe. Situation for SNe pseudotypes independent case.

Table 8. Statistic parameters of distribution of size of errorbox for long and short GRBs.

	$T_{90} < 2 \text{ s}$	$T_{90} > 2 \text{ s}$
count	497	1540
minimum	0.63°	0.09°
median	6.10°	2.33°
maximum	23.09°	26.56°
mean value	6.77°	3.15°
standard deviation	4.05°	2.84°

4.4.2. Results

For \mathbb{A} set the ratio between the number of the short and the long GRBs in the match $R_{\mathbb{A}} \equiv N_{\text{short}}/N_{\text{long}} = 1.057$, for \mathbb{B} it yields $R_{\mathbb{B}} = 1.023$. However, this ratio for all GRBs in the whole BATSE catalogue (for the burst with T_{90} defined) yields $R_{\text{all}} = 0.323$.

The relative number of short GRBs in the sub-sample of the GRBs possibly correlated with SNe is three times higher than in the whole GRB catalogue (see Fig. 9).

This result is rather misleading. The answer is hidden in the fact that the short GRBs are harder where the anti-correlation between the hard to soft ratio and the duration T_{90} is clearly seen (Kouvelioutou 1993). The harder spectrum influence on the preciseness of the localization and thus the short GRBs have larger errorboxes in average. The statistical properties of the GRB errorbox distribution are listed in Table 8 (see the Fig. 10). This means that the probability of a match should take into account the size of the errorbox. This is the reason for higher abundance of the short GRBs in the real match in comparison to the random case simulated by a set of the rotation tests. This argument is demonstrated in Fig. 9.

The sum of the abundance of the short and the long GRBs normalized to the number of all GRBs is not equal exactly to unity, because there are a few GRBs which repeat in the sample due to multiple coincidence in the match and a few GRBs are provided with no T_{90} information. This is also a reason why the mean relative abundances of GRBs of one sort are not in the same ratio of the mean surfaces of errorboxes.

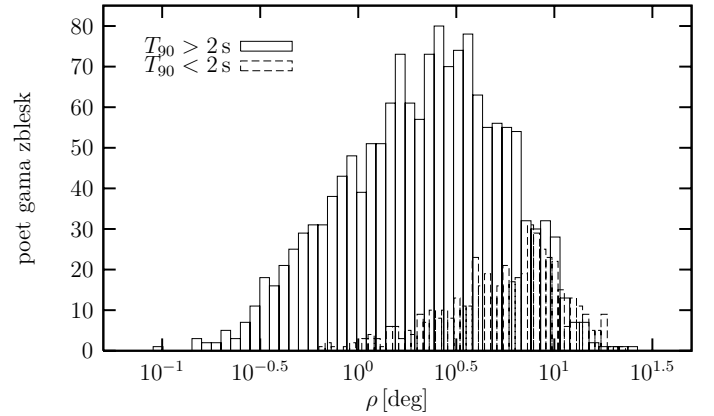


Fig. 10. Distribution of size of errorbox ρ for long and short GRBs.

4.5. Kolmogorov-Smirnov

4.5.1. Theory

An interesting question is whether the fraction f of physically correlated (if there is any correlation) SNe and GRBs differs from the rest of the sample of their kind, or not. If they do, the sub-sample of the possibly correlated SNe and GRBs will show the excess against the whole sample in the meaning of the difference between the cumulative distribution functions (CDFs) of the sets. We investigated it using Kolmogorov-Smirnov (KS) test.

We tested the following properties of GRBs: the duration T_{90} , the fluences f_2 and f_3 , the hard to soft (h2s) ratio defined as f_3/f_2 and the errorbox radius ρ and, the following properties of SNe: the absolute and apparent visual magnitude M and m , the redshift z and offset from the host galaxy r .

4.5.2. Results

The results of the KS test are shown in Table 9 for SNe and in Table 10 for GRBs, the numbers of objects available for the analysis are included. They are also plotted in the Fig. 12 for SNe. The lower boundary of the validity of the KS test is at least ~ 80 objects in the data set to give significant results. It not always fulfilled (e.g. in the case \mathbb{A} the number of the objects for some quantities is $N \sim 50$ only).

Note, that all the SNe in the catalogue are relatively close SNe with the median $z_{\text{SN}} = 0.02$ (and the mean value is $\bar{z}_{\text{SN}} = 0.12$) and the distance up to $z_{\text{SN}} = 1.70$. The median of the distance distribution of all GRBs, for which the redshift is known, is $z_{\text{GRB}} \sim 1$ (Greiner 2004). If there are some physically related pairs among the possibly correlated matched pairs they come from relatively nearby Universe and they are less affected by the cosmological effects (Hubble expansion). Thus they should be brighter, shorter and harder than the average class member in the statistical meaning (Fenimore & Bloom 1995) (e.g. GRB 030329 is not shorter neither harder e.g. GRB 030329 at $z = 0.169$ is not shorter neither harder).

Although, as seen from the Fig. 11, the GRBs from the matched pairs are harder and shorter than the average, but the F_{64} of these GRBs is not higher than the average. We conclude that the higher abundance of the harder and shorter GRBs among the possibly correlated matched ones is due to the selection effect caused by relatively larger errorboxes of short GRBs. The influence of the size of the errorbox is discussed above.

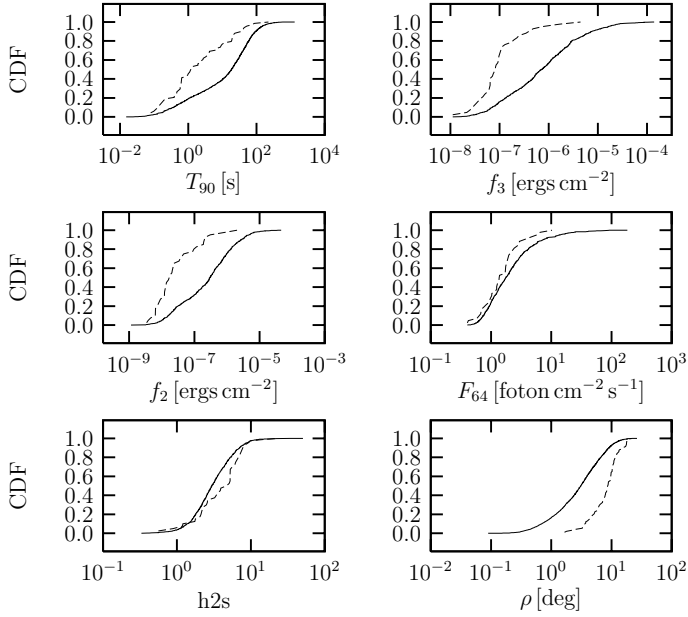


Fig. 11. Differences of CDF of chosen parameters of GRBs. Dashed lines are for matched GRBs, solid for whole population. Situation for SNe pseudotypes independent matching.

Table 9. Results of KS test of SNe physical parameters (most correlated).

quantity	KS(A)	N(A)	KS(B)	N(B)
M	6.50×10^{-1}	78	5.81×10^{-1}	104
d_L	1.78×10^{-1}	79	8.34×10^{-3}	105
z	1.78×10^{-1}	79	8.34×10^{-3}	105
m	1.93×10^{-1}	91	6.51×10^{-1}	126
r	2.43×10^{-1}	63	2.53×10^{-1}	79

Table 10. Results of KS test of GRBs physical parameters (most correlated).

quantity	KS(A)	N(A)	KS(B)	N(B)
T_{90}	4.77×10^{-9}	68	2.49×10^{-10}	90
f_3	4.85×10^{-12}	43	0.00	62
f_2	4.63×10^{-10}	43	8.44×10^{-15}	62
F_{64}	6.54×10^{-2}	43	4.08×10^{-3}	62
$h2s$	4.38×10^{-3}	40	8.23×10^{-4}	60
ρ	0.00	92	0.00	127

4.6. Relative abundance of pseudotypes

4.6.1. Theory

As it was already mentioned, according to the hypothesis of the GRB-SN connection the physical correlation – if any – between GRBs and SNe is expected for the core SNe only. We studied the spectrum of SN pseudotypes in the set of the possibly correlated SNe with respect to all SNe. We tested whether the relative abundance of the core SNe differs from the whole SN catalogue and whether it differs from the results when artificially created catalogues were used.

4.6.2. Results

The spectra of the pseudotypes both for the cases A and B of the match are shown in Table 1. The total number of objects is related to the BATSE era. Because we have the multi-matched

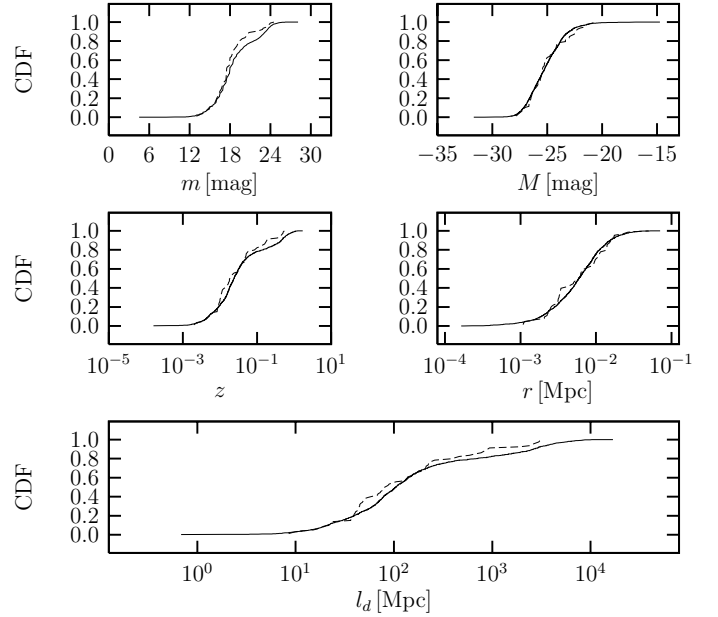


Fig. 12. Differences of CDF of chosen parameters of SNe. Dashed lines are for matched SNe, solid for whole population. Situation for SNe pseudotypes independent matching.

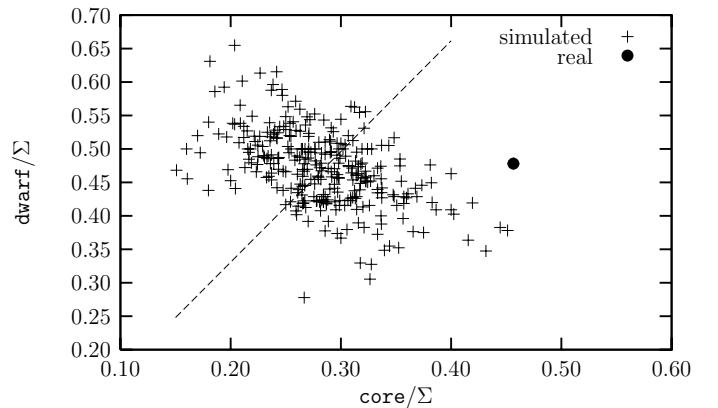


Fig. 13. Fraction of core and dwarf SNe pseudotypes in matched pairs. Dashed line respect fraction in whole population of SNe. Situation for SNe pseudotypes independent matching.

SNe among the matched pairs, the number of the matched SNe differs from the number of the matched pairs. First we neglect the unknown SNe and we compare the relative number of the core SNe to the relative number of the dwarf SNe among the matched ones. We see that the relative abundance of the core SNe is more than twice as high as the relative abundance among all SNe in the catalogue. Note, that the angular distribution of the dwarf and the core SNe is not significantly different.

To exclude the various possible selection effects and to prove the higher number of the core SNe among the coinciding pairs we compare the results of the real match with artificially random SN and GRB distribution we can generate using the rotation method again.

In the case of artificially built catalogues we see a significant difference between the A and B sets of parameters. This is due to the different size of the time window in the case A, where the core SNe are preferred by a larger size of the time interval. If we correct the results for the different size of the time interval,

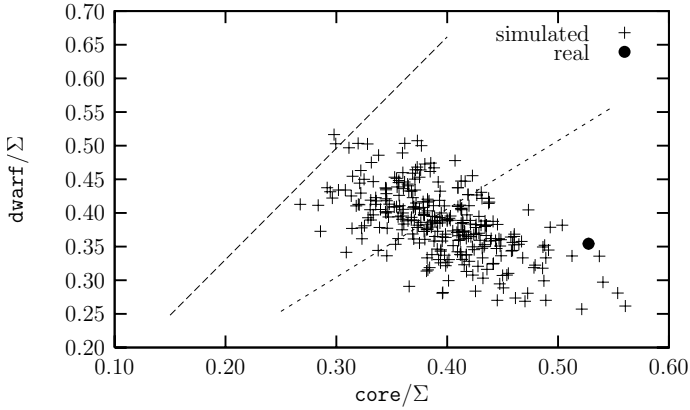


Fig. 14. Fraction of core and dwarf SNe pseudotypes in matched pairs. Left dashed line respect fraction of whole SNe population. Right dashed fraction correct fraction of whole SNe population by different core and dwarf time window size. Matching respect SNe pseudotypes.

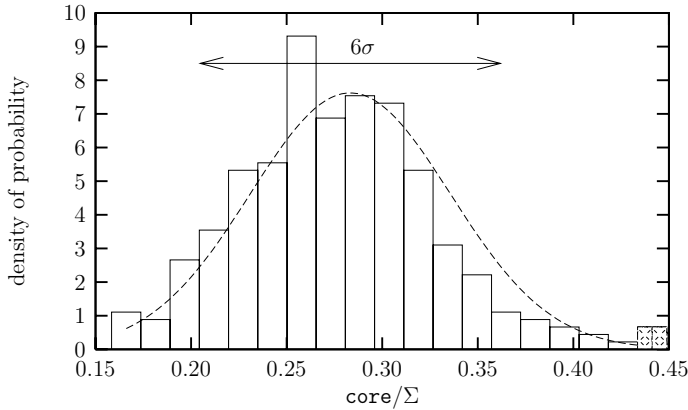


Fig. 15. Histogram of fraction of core SNe pseudotype in matched pairs (x -axis in Fig. 13). Filled box on right side contains fraction in real match. Situation for SNe pseudotypes independent matching.

using the weighted average of the the size of the time window, the discrepancy becomes minimal.

However, the relative abundancy of the core SNe in the real match still remains different from the distribution of the relative abundances in the random cases. The distribution of the abundances of the core SNe in the artificial data set is Gaussian up to 97.8% in the meaning of KS test and the relative abundancy of the core SNe in the real match is out of 3σ interval. It is interesting to mention, that the relative abundancy of the dwarf SNe in the real match is approximately the same as in the random case. The higher relative number of core SNe in the real match is to the prejudice of the unknown SNe.

It may be a consequence of the real physical correlation between the GRBs and core SNe or we encounter another version of a selection effect, namely the hypothesis that the suspicious SNe which are located in the vicinity of a GRB were inspected more carefully than the others.

4.6.3. Ib/c pseudotype

Apart from the analysis of the relative abundancy of the major (dwarf and core) pseudotypes we can test for the minor pseudotypes as well. The most discussed type of SNe, possibly physically correlated with GRBs in general, is the type Ib/c (Berger et al. 2003). Our result is shown in the Fig. 16.

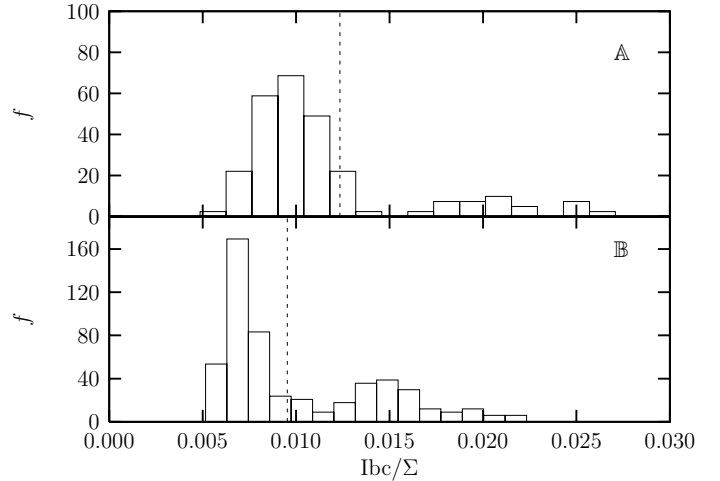


Fig. 16. Relative abundance of pseudotype Ib/c. Dashed lines shows abundance in real match.

Unfortunately the number of the objects among the matched pairs is too small to say any considerable conclusion. For a more detailed discussion of the results of the Ib/c abundancy among the matched pairs according to a recent revision of Ib/c SNe (Berger et al. 2003) see (Topinka & Polcar 2006).

4.7. Isotropic energy equivalent

Assuming that the matches are due to the real correlation and assigning redshift of the SN to the GRB for every matched pair we can derive corresponding GRB isotropic energy equivalent (IEE) radiated in gamma-rays (using standard cosmology parameters $H_0 = 70 \text{ km s}^{-1} \text{ Mpc}^{-1}$, $\Omega_m = 0.3$, $\Omega_\Lambda = 0.7$). The peak of the distribution of IEE for matched pairs is similar to the IEE of SN 1998bw $\sim 8 \times 10^{47} \text{ erg}$ (Fig. 17). But IEE is more sensitive to the redshift variations than to the fluence variations, thus a relatively narrow redshift distribution can cause the accumulation of values around the value derived for average GRB fluence at an average SN distance. We can hence deduce that there may be other unrevealed SN 1998bw-like among the BATSE GRBs. However the IEE distribution for the real match is *not* significantly different from the one for the random match. The number of the pairs matched due to the physical link is below the level of resolution of such a test. It could also mean that coincidence between SN 1998bw and GRB 980425 was just accidental one.

The mean IEE of matched GRBs is four orders of magnitude lower than the average GRB IEE, which means that assuming their connection with the matched SNe we most probably underestimate their distances and thus the connection is not real for most of the matched pairs.

5. Conclusion

We have performed the search for the correlation between BATSE GRBs and SNe. All the results depend on the validity of the matching condition. If the matching criteria are at least partly valid then the obtained results are relevant.

We found 92 possibly matched pairs of a GRB and a SN for the SN type dependent on matching criteria (the case A) and 127 pairs for the matching independent on the SN type (the case B).

All the results were tested whether they are normal or they show an excess from the random distribution of the objects of

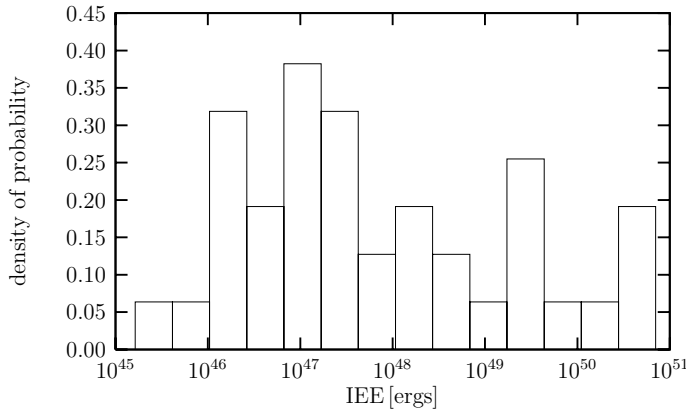


Fig. 17. Distribution of IEE of matched GRBs. Situation for SNe pseudotypes independent case.

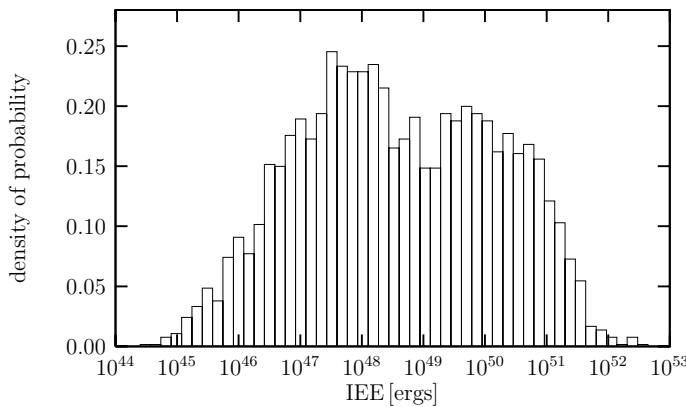


Fig. 18. Distribution of IEE of random (rotate GRBs coordinates) matched GRBs. Situation for SNe pseudotypes independent case.

the same type. We artificially generated the random catalogues with the desired statistical properties, e.g. with the same statistical properties as the real catalogues, using the technique of catalogue rotation.

There is an upper limit for the fraction of the number of physically correlated GRBs and SNe of order of a few per cent. From the analysis of the number of the matched pairs we can conclude that if there ever exists any correlation between BATSE GRBs and SNe it is smaller than this limit.

If one assumes that GRBs are highly collimated and that there is a corresponding GRB to every detected (spherically exploding) SN – even when the GRB is not observed for the reason that the GRB jet “misses” a detector – we can put the upper constraint on the size of the GRB jet angle. Assuming the BATSE sky coverage about 50% we get the maximal jet-size of around $\theta = 17$ deg from the resolution limits of our match tests. It is within the range of generally accepted values (Friedman & Bloom 2004)

Even in the case of a real correlation the physical properties of the GRBs from the sample of the matched GRBs would not be significantly different from the rest of all GRBs, i.e. none of the physical properties of the sample of the possibly correlated SNe would be significantly different from the rest of all SNe in the meaning of KS test. Neither the closer study of GRB energy distribution indicated any hint for real correlation. Although the IEE of GRB980425 fits well into general IEE distribution it is not relevant within the framework of the tests we did. If there is any it smeared out due to the quite low fraction of physically correlated pairs.

We searched for the correlation among physical properties of the suspicious objects within the pairs, but neither positive nor negative correlation was found.

An interesting result comes from the spectrum of the SN pseudotypes. There is a higher abundance of the core SNe originating from the core-collapse than in the average SNe distribution in the meaning of 3σ . The possibility of the influence of the selection effect by the size of error boxes was excluded.

There is also a higher abundance of type Ib/c SNe among the matched pairs, but the size of the sample is statistically small.

Acknowledgements. We acknowledge the support by the Grant Agency of the Academy of Sciences of the Czech Republic, grant A3003206 and 205/03/H144.

References

- Berger, E., Kulkarni S. R., Frail, D. A., & Soderberg, A. M. 2003, ApJ, 599, 408
van den Bergh, S., Tammann, G. A. 1991, Galactic and extragalactic supernova rates IN: Annual review of astronomy and astrophysics (Palo Alto, CA: Ann. Rev., Inc.), 29, 363
Blinnikov, S., Lundqvist, P., Bartunov, O., Nomoto, K., & Iwamoto, K. 2000, ApJ, 532, 1132
Bloom, J. S., Kulkarni, S. R., Djorgovski, S. G., et al. 1999, Nature, 401, 453
Bloom, J. S., Kulkarni, S. R., & Djorgovski, S. G. 2002, AJ, 123, 1111
Bloom, J., Blake, C., Prochaska, J. X., et al. 2005, GCN observation report #3388
Colgate, S. A. 1974, ApJ, 187, 333
Dar, A. 2004, The GRB/XRF-SN Association [arXiv:astro-ph/0405386]
Drago, A. 2000, Understanding Deconfinement in QCD, 342
Fenimore, E. E., & Bloom, J. S. 1995, ApJ, 453, 25
Frail, D. A., Kulkarni, S. R., Sari, R., et al. 2001, ApJ, 562, L55
Friedman, & Bloom, 2004 [arXiv:astro-ph/0408413]
Galama, T. J., Wijers, R. A. M. J., Bremer, M., et al. 1998, ApJ, 500, 97
Galama, T. J., Tanvir, N., Vreeswijk, P. M., et al. 2000, ApJ, 536, 185
Greiner's web page: <http://www.mpe.mpg.de/~jcg/>
Hjorth, J., Sollerman, J., & Møller, P. 2003, Nature, 423, 847
Hudec, R. 1999, Acta Historica Astronomiae, 6, 28
Hudec, R., Hudcova, V., & Hroch, F. 1998, A&AS, 138, 475
Hudec, R., Hudcova, V., Palazzi, E., Masetti, N., & Pizzichini, G. 2001, in Exploring the gamma-ray universe, Proceedings of the Fourth INTEGRAL Workshop, 4–8 September 2000, Alicante, Spain, ed. B. Batrick, Scientific ed. A. Gimenez, V. Reglero, & C. Winkler (Noordwijk: ESA Publications Division), ESA SP-459, 387
Jakobsson, P., Hjorth, J., Fynbo, J. P. U., et al. 2004, ApJ, 617, L21
Ruffert, M., & Janka, H.-T. 1999, Gamma-Ray Bursts: The First Three Minutes, ASP Conf. Ser., 190, 181
Kippen, R. M., Briggs, M. S., Komers, J. M., et al. 1998, ApJ, 506, L27
Koshut, T. M. 1996, Ph.D. Thesis
Kouvelioutou 1993, ApJ, 413, L101
MacFayeden, A. I., & Woosley, S. E. 1999, ApJ, 524, 262
Madau, P. 1998, Galaxy Evolution and the Cosmic Rate of Supernovae, in The Young Universe: Galaxy Formation and Evolution at Intermediate and High Redshift, ed. S. D'Odorico, A. Fontana, & E. Giallongo, ASP Conf. Ser., 146, 289
Malesani, D., Tagliaferri, G., Chincarini, G., et al. 2004, ApJ, 609, L5
Matheson, T. 2004 [arXiv:astro-ph/0410668]
Metger, M. R., Djorgovski, S. G., Kulkarni, S. R., et al. 1997, Nature, 387, 878
Paczynski, B. 2001, Supernovae and Gamma-Ray Bursts: the Greatest Explosions since the Big Bang, 1
Petschek, A. G. 1996, Supernovae (New York: Springer Verlag)
Piro, et al. 2000, Science, 290, 956
Press, W. H., Flannery, P., Teukolsky, S. A. N., Vetterling, W. T. 1968, Numerical Recipes (Cambridge University Press)
Rees, M. J., & Meszaros, P. 1992, MNRAS, 258, 41P
Stanek, K. Z., Matheson, T., Garnavich, P. M., et al. 2003, ApJ, 591, L17
Topinka, M., & Polcar, J. 2006, in preparation
Tsvetkov, D. Y., Blinnikov, S. I., & Pavlyuk, N. N. 2001, Astron. Lett., 27, 411
Vietri, M., & Stella, L. 1998, ApJ, 507, L45
Wang, L., & Wheeler, J. C. 1998, ApJ, 504, L87
Woosley, S. E. 1993, ApJ, 405, 273
Gal-Yam, et al. 2003, ApJ, 609, L59
Zeh, A., Klose, S., Hartmann, D. H., et al. 2004, ApJ, 609, 952
Zeh, A., Klose, S., Hartmann, D. H., et al. 2005 [arXiv:astro-ph/0503311]